Synthesis of Novel Silicon-Containing Amphiphilic Diblock Copolymers and Their Self-Assembly Formation in Solution and at Air/Water Interface

Kozo Matsumoto,* Utako Mizuno, Hideki Matsuoka,* and Hitoshi Yamaoka†

Department of Polymer Chemistry, Kyoto University, Kyoto 606-8501, Japan

Received July 17, 2001; Revised Manuscript Received October 29, 2001

ABSTRACT: Amphiphilic block copolymers, poly(1,1-dimethylsilacyclobutane-*block*-2-hydroxyethyl methacrylate) (poly(DMSB-*b*-HEMA)), poly(1,1-diethylsilacyclobutane-*b*-2-hydroxyethyl methacrylate) (poly(DESB-*b*-HEMA)), and poly(1,1-dibutylsilacyclobutane-*block*-2-hydroxyethyl methacrylate) (poly(DBSB-*b*-HEMA), were synthesized by a living anionic polymerization, and their self-assembled structures were investigated. Small-angle X-ray scattering (SAXS) analysis suggested that the block copolymers formed micelles in methanol and that the aggregation number of the micelles increased with the increase of polysilacyclobutane (polySB) content and number of carbon atoms in the alkyl groups on silicon. A remarkable temperature dependence of the micelle structure of poly(DMSB-*b*-HEMA) was observed. Small-angle neutron scattering (SANS) revealed that the block copolymer formed spherical micelle with a core−shell structure above room temperature and a disklike micelle below room temperature. The surface pressure−area per molecule ($\pi-A$) isotherm of spread copolymer indicated that poly(SB-*b*-HEMA)s formed a thin layered film on the water surface. The $\pi-A$ isotherm of the poly(DMSB-*b*-HEMA) spread layer also exhibited a characteristic temperature dependence. Direct X-ray reflectivity (XR) measurement on the water surface indicated that the block copolymers formed a monolayer with uniform thickness and smooth interfaces at medium surface pressure around 30 mN/m. In the case of poly(DBSB-*b*-HEMA), on the other hand, it was supposed that another layer with a large thickness appeared in the monolayer at a higher surface pressure than 35 mN/m. Atomic force microscopy (AFM) measurement of poly(DBSB-*b*-HEMA) film deposited on a glass plate at that surface pressure supported the existence of a thicker layer in addition to monolayer.

Introduction

Amphiphilic block copolymer has attracted keen attention[1,2] because it can form various nanostructures such as micelles[3−5] by self-assembling in the selective solvent or monolayers[6−8] by adsorption at the air−liquid interface. Structures of the micelles and monolayers strongly depend on the hydrophilic−lipophilic balance and polymer architecture as well as the polymer concentration, salt concentration, temperature, solvent pH, and so on. To comprehensively investigate the self-assembling behavior of amphiphilic block copolymers, it is necessary to prepare polymer samples with well-controlled molecular weight of hydrophobic and hydrophilic segment with a narrow molecular weight distribution and sufficiently high chemical stability.

Silacyclobutane (SB), a silicon-containing four-membered ring compound, can be polymerized in a living manner to afford a hydrophobic, chemically stable, and highly flexible silicon-containing polymer.[9] Recently, we have developed and established a living anionic ring-opening polymerization of 1,1-dialkylsilacyclobutanes.[10] As a result, preparation of block copolymer of SB with other monomers such as methacrylic esters along with controlled molecular weight and narrow molecular weight distributions is now possible.[11] Another important advantage of the SB monomer is its wide synthetic versatility. Various organic groups can be readily introduced on the silicon atom and the monomer can be polymerized with a living nature.[12] Therefore, SB is particularly expected to be a highly useful monomer in the detailed investigation on self-organization of amphiphilic block copolymers.

We have already reported preliminary results on the micelle[13] and monolayer[14] formation of amphiphilic block copolymers composed of poly(1,1-diethylsilacyclobutane) and poly(2-hydroxyethyl methacrylate). In this study, we synthesized a series of amphiphilic block copolymers composed of polySB with methyl, ethyl, and butyl groups on silicon atoms as a hydrophobic segment and poly(2-hydroxyethyl methacrylate) (polyHEMA) as a hydrophilic segment. Then we examined the effect of the chain length of polySB segment and the substituent at silicon atoms on the micelle formation in methanol by small-angle X-ray scattering (SAXS) and small-angle neutron scattering (SANS). We also investigated the structure of the polymer monolayer formed at the air−water interface by surface pressure measurement, in situ X-ray reflectometry (XR),[15] and atomic force microscopy (AFM) measurement of the film deposited on a glass plate.

Experimental Section

Materials. 1,1-Dichlorosilacyclobutane was purchased from Aldrich (Mirwaukee, WI) and used as delivered. 1,1-Dimethylsilacyclobutane (DMSB) was purchased from Shin Etsu (Tokyo, Japan) and distilled twice under reduced pressure over CaH_2. 1,1-Diethylsilacyclobutane (DESB) and 1,1-dibutylsilacyclobutane (DBSB) were prepared by treatment of 1,1-dichlorosilacyclobutane and ethylmagnesium bromide or butylmagnesium bromide in THF at 0 °C and purified by distillation under reduced pressure over lithium aluminum hydride. 1,1-Diphenylethylene was purchased from Tokyo Chemical Industry (Tokyo, Japan) and distilled from butyllithium in a vacuum. 2-(*tert*-Butyldimethylsiloxy)ethyl methacrylate (Si-HEMA) was prepared according to the reported procedure[16] and purified by distillation under reduced pressure

* To whom correspondence should be addressed.

† Present address: Department of Materials Science, Faculty of Engineering, University of Shiga Prefecture, 2500 Hassaka, Hikone 522-8533, Japan.

10.1021/ma011254n CCC: $22.00
Published on Web 12/18/2001

over CaH_2. Butyllithium hexane solution (1.6 M) was purchased from Wako (Osaka, Japan) and diluted with dry hexane. Phenyllithium diethyl ether solution (1.0 M) was purchased from Kanto Chemicals (Tokyo, Japan) and used as delivered. Lithium chloride was purchased from Wako and dried by heating for 3 h at 130 °C in a vacuum. Tetrahydrofuran (THF) and hexane were freshly distilled over sodium benzophenone ketyl in an argon atmosphere before use. Lithium naphthalene was prepared by treatment of naphthalene with lithium metal in THF.

Sample Preparation. To a 50 mL two-necked, round-bottomed flask equipped with a three-way stopcock, a rubber balloon, a rubber septum, and a magnetic stirring bar were charged lithium chloride (0.35 M THF solution, 1.0 mL, 0.35 mmol), THF (5 mL), and hexane (4 mL) in an argon atmosphere. The solution was titrated with a THF solution of lithium naphthalene to eliminate a trace amount of reactive impurities. An initiator solution (1.0 M 0.25 mL, 0.25 mmol, butyllithium hexane solution for DMSB, phenyllithium diethyl ether solution for DESB and DBSB) and a monomer (DMSB, DESB, or DBSB, 2.5−5.0 mmol) were added at −48 °C, and the reaction mixture was stirred for 20 min for DMSB, 60 min for DESB, and 120 min for DBSB. To the solution thus prepared was added 1,1-diphenylethylene (0.09 mL, 0.50 mmol), and the mixture was stirred for 30 min. Then Si-HEMA (5.0−10.0 mmol) was introduced, and the mixture was stirred for another 1 h. The polymerization was terminated by addition of methanol (0.5 mL). The resulting products were precipitated by putting into excess methanol, filtered out, and dried to give poly(SB-*b*-Si-HEMA). To obtain copolymers with different block ratios, the amount of each monomer was varied.

The copolymers were hydrolyzed with diluted hydrochloric acid (3.0 M, 1.0 mL) in 1,4-dioxane (12 mL) at room temperature for 24 h and led to poly(DMSB-*b*-HEMA), poly(DESB-*b*-HEMA), and poly(DBSB-*b*-HEMA). The products were purified by dialysis against ultrapure water (Milli-Q, Millipore, Bedford, MA) to give a white precipitate, which were filtered out and dried in vacuo.

Characterization of Block Copolymers. Gel permeation chromatography was carried out in chloroform on a JASCO 880-PU chromatograph (JASCO Engineering, Tokyo, Japan) equipped with four polystyrene gel columns (Shodex K-802, K-803, K-804, and K-805; exclusion limit in molecular weight of polystyrene = 5×10^3, 7×10^4, 4×10^5, and 4×10^6, respectively) and a JASCO 830-RI refractive index detector. The molecular weight distributions (M_w/M_n) were determined relative to polystyrene standards. Proton NMR spectra were recorded on a JEOL GSX 270 spectrometer in $CDCl_3$ or CD_3OD. The number-average polymerization degrees of polyDMSB, polyDESB, polyDBSB, and polyHEMA segments were determined by the integral ratios of ^1H NMR signals in each segment to those of the initiation end groups. Molecular characterizations of the block copolymers were performed before hydrolysis, since the precursor polymers were molecularly dissolved in chloroform, which is the solvent in NMR and the eluent of GPC. We confirmed by ^1H NMR that no side reaction had taken place during hydrolysis.

Differential Scanning Calorimetry (DSC) Measurements. The DSC measurements were performed on MAC Science DSC 3100 (Mac Science, Yokohama, Japan) at −100 to +100 °C using 5 mg polymer samples sealed in an aluminum container and found to be reproducible with no apparent hysteresis over three heating and two cooling scans at a rate of 10 °C/min. α-Alumina was used as a standard.

Small-Angle X-ray Scattering (SAXS). The SAXS measurements were performed using a Kratky type camera (Rigaku Corp, Tokyo) equipped with a rotating anode X-ray generator and a position sensitive proportional counter (PSPC). The details of the apparatus and data treatment were fully described elsewhere.[17] Polymer solutions were prepared by direct dissolution of the block copolymer into methanol and heating once up to 50 °C and filtrated through a membrane (Millex-GV, Millipore, pore size of 0.22 mm) and then cooling to an ambient temperature. In all measurements, the polymer concentration was 1 wt %. Sample solutions were measured in glass capillaries (Mark, Berlin) with a diameter of 2 mm. The typical accumulation time of a SAXS run was about 2 h. In experimental data, the scattering from methanol was subtracted.

Small-Angle Neutron Scattering (SANS). The SANS measurements were performed by SANS-U of the Institute for Solid State Physics, The University of Tokyo, at the research reactor JRR-3, Tokai, Japan. The wavelength (λ) of neutron beam was 7 Å ($\delta\lambda/\lambda = 10\%$). Solutions were measured in the quartz cells (Nippon Silica Glass Co., Tokyo) with a pass length of 4 mm. Scattering data measured by a 2D detector were circular averaged to 1D and then corrected for electronic background, and the scattering of the empty cell was subtracted. The data were transformed to absolute intensities using the Lupolen standard. From all scattering data of samples, we subtracted the scattering of solvent and the calculated incoherent scattering of the polymer. The SANS experiments were carried out at sample−detector distances of 1, 4, and 12 m, covering a range of the scattering vector (q) of $0.003 \le q \le 0.28$ Å^{-1}. We used CD_3OD as a solvent and 1 wt % polymer solutions for all measurements. The typical accumulation times of SANS runs were 20 min (for 1 m sample−detector distance), 0.5 h (for 4 m), and 2.5 h (for 12 m).

Data Analysis of SAXS and SANS Measurements. A similar basic principle can be applied for both SAXS and SANS analysis. The main difference is that the neutron is scattered by the density fluctuation of scattering length, while the scattering of X-ray occurs by the electron density fluctuation.

When the contribution of interparticle interaction is negligible, the scattering cross section is given by the equation

$$d\Sigma(q)/d\Omega = n_p P(q) \tag{1}$$

where n_p is the number density of particles and $P(q)$ is the particle form factor. The scattering vector q is defined by $q = 4\pi \sin\theta/\lambda$, where 2θ is the scattering angle and λ is the wavelength of neutron or X-ray. Here we deal with the micelles having a core−shell structure with the homogeneous electron density in the core and the shell regions. In such a model, polySB forms the core, and the shell contains polyHEMA hair and the solvent. The particle form factor of a core−shell model can be written as follows:

$$P(q) = (1/2)\int_0^{\pi}\{(\rho_C - \rho_S)V_C F_C(q) + (\rho_S - \rho_0)V_S F_S(q)\}^2 \sin\beta \, d\beta \tag{2}$$

where ρ_C, ρ_S, and ρ_0 are the scattering length densities (for SANS) and electron densities (for SAXS) of the core, the shell, and the solvent, respectively. V_C and V_S are the volumes of the core and overall micelle, respectively. The scattering amplitude $F_i(q)$ (i = c, s, c denotes the core and s the shell) depends on the size and shape of the scattering particles. For a monodisperse isolated sphere with a radius of R_i, $F_i(q)$ is given by

$$F_i(q) = 3(\sin(qR_i) - qR_i\cos(qR_i))/(qR_i)^3 \tag{3}$$

Using the value of the electron density of the monomer unit ρ_{SB} and ρ_{HEMA}, ρ_c and ρ_s can be represented by

$$\rho_c = \rho_{SB} \tag{4}$$

$$\rho_s = \phi_{sol}\,\rho_0 + (1 - \phi_{sol})\rho_{HEMA} \tag{5}$$

where ϕ_{sol} is the volume fraction of the solvent in the shell, which can be calculated by the following equation with the degree of polymerization of HEMA (m), the volume of HEMA repeating units (ν_{HEMA}), the volume of the core (V_c), and the volume of the overall micelle (V_s):

$$\phi_{sol} = 1 - N_{agg} m \nu_{HEMA}/(V_s - V_c) \tag{6}$$

N_{agg} denotes the aggregation number of the micelles, which is calculated from V_c, the degree of polymerization of SB (n), and the volume of SB repeating units (n_{SB}):

$$N_{agg} = V_c/(n\nu_{SB}) \tag{7}$$

Assuming that all polymers contribute to the micelle formation, the number density n_p of the micelles is then calculated:

$$n_p = \phi/(N_{agg}(n\nu_{SB} + m\nu_{HEMA})) \tag{8}$$

where ϕ is the volume fraction of copolymer in solution.

When the polydispersity in micelle size is taken into account, the form factor is given by

$$\langle P(q)\rangle = \int_0^\pi G(R)\, P(q,R)\, dR \tag{9}$$

We assume that the size distribution is given by a Gaussian function $G(R)$

$$G(R) = (2\pi)^{-1/2}{\sigma_{R_s}}^{-1} \exp[-(R - R_s)^2/2{\sigma_{R_s}}^2] \tag{10}$$

where R_s and σ_{R_s} are the average and the standard deviation of micellar size, respectively.

For a disklike structure with a core thickness of L_C, the overall micelle size L_S, and radius R_{Disk}, the scattering amplitude is given by

$$F_i(q) = \{(\sin(q(L_i/2)\cos\beta))/(q(L_i/2)\cos\beta)\} \times \{2J_1(qR_{Disk}\sin\beta)/(qR_{Disk}\sin\beta)\} \tag{11}$$

where β is the angle between the axis of symmetry of particle and the scattering vector q, J_1 denotes the Bessel function of the first kind and of the order 1, and i represents c or s. If R_{Disk} is much larger than L_i, formula 11 can be reduced to

$$F_i(q) = \{\sin(qL_i/2)/(qL_i/2)\}/(qR_{Disk})^2 \tag{12}$$

For SAXS data analysis, we introduced a shift factor f, since the intensity of the experimental data is obtained in arbitrary units because the data have not been calibrated to an absolute scale. Therefore, the relative scattering intensity $I(q)$ is given by

$$I(q) = fn_pP(q) \tag{13}$$

The electron densities of $\rho_{DMSB} = 0.279$, $\rho_{DESB} = 0.280$, $\rho_{DBSB} = 0.286$, $\rho_{HEMA} = 0.396$, and $\rho_0 = 0.268$ Å^{-3} and the scattering length density of $\rho_{DMSB} = -3.73 \times 10^9$, $\rho_{HEMA} = 1.12 \times 10^{10}$, and $\rho_0 = 5.81 \times 10^{10}$ cm^{-2} were fixed, which were calculated from electron number or scattering length in each monomer unit, unit formula weight, and bulk density of each monomer and solvent. The bulk densities of 0.827 g/cm^3 for polyDMSB, 0.828 g/cm^3 for polyDESB, 0.841 g/cm^3 for polyDBSB, and 1.17 g/cm^3 for polyHEMA were used. In the core−shell model fitting, three parameters, R_c, R_s (or L_c, L_s), and f were variable, while the value of f was arranged to be the same in each measurement sequence.

For the sphere−disk coexistence model, the scattering intensity is given by

$$d\Sigma(q)/d\Omega_{sphere-disk} = n_p\phi_{Nsphere}P(q)_{sphere} + n_p\phi_{Ndisk}P(q)_{disk} \tag{14}$$

where $\phi_{Nsphere}$ and ϕ_{Ndisk} are number fractions of the sphere and disk micelles in the total number of micelles in the solution, and $P(q)_{sphere}$ and $P(q)_{disk}$ are form factors of the corresponding micelles. Equation 14 can be written as follows:

$$d\Sigma(q)/d\Omega_{sphere-disk} = (m_p\phi_{sphere}/N_{sphere})P(q)_{sphere} + (m_p\phi_{disk}/N_{disk})P(q)_{disk} \tag{15}$$

where m_p is number density of polymer molecules, ϕ_{sphere} and ϕ_{disk} are volume fractions of the micelles in the total volume of micelles, and N_{sphere} and N_{disk} are the aggregation numbers of the sphere and disklike micelles.

***π*−*A* Measurement.** A surface pressure (π)−surface area (A) isotherm of a spread monolayer was obtained with a trough (length 600 mm × width 150 mm) made of aluminum coated by Teflon equipped with a film balance controller FSD-220 (USI System, Fukuoka, Japan). The water used as subphase was ultrapure water obtained by a Millipore Milli-Q system. The copolymer was first dissolved in chloroform to make a 1.0 mg/mL solution and then spread on the water surface by a microsyringe to prepare a monolayer. Before surface compression was started, 30 min was allowed for solvent evaporation. The surface layer was compressed by moving a Teflon barrier at the rate of 0.1 mm/s.

X-ray Reflectivity (XR) Measurement. The XR measurements were performed by a RINT-TTR-MA (Rigaku Corp., Tokyo, Japan) which was constructed by a modification of the RINT-TTR $\theta-\theta$ rotating anode X-ray system for reflectivity measurement. The details of the XR apparatus and data treatment have been fully described previously.[7b,18] The advantage of this apparatus is that in situ measurement for the monolayer at the air−water interface is possible since the angle scanning measurement can be performed by rotation of both the X-ray source and the detector; it is not necessary to rotate the sample during measurement. In addition, a specially designed trough (length 80 mm × width 60 mm) with a barrier made of Teflon (USI System, Fukuoka, Japan) is mounted on the sample stage, which makes possible the XR measurements of a monolayer on water with the change of surface pressure. The wavelength of the incident X-ray (λ) is 1.5406 Å (Cu Kα_1). The measurements were performed under a specular condition; i.e., the incident and reflection angles were equal (θ). The reflectivity was obtained as a function of the scattering vector q ($= 4\pi \sin q/\lambda$).

The trough for XR was washed with chloroform and methanol and dried before the water was fulfilled. Cleanness of the water surface was confirmed by obtaining a satisfactory isotherm of the clean water surface: no increase of surface pressure by compression. The chloroform solution of the copolymer that was used for $\pi-A$ measurement was spread on the water. The XR profiles were obtained at 28 °C ∼ 29 °C at the surface pressures of 20, 25, 30, 35, and 40 mN/m. Each XR measurement took about 1 h to obtain the whole profile. Calculation and data analysis for XR were carried out using a scientific software program invented by Rigaku Corp. and the scientific program "MUREX118 (Multiple Reflection of X-rays)".[19] The procedure of data fitting and simulation is based on the theory of Parratt[20] and Sinha et al.[21] To analyze XR data, we assumed a two-layer model in which the upper layer (first layer) is composed of hydrophobic polySB and the lower layer (second layer) of hydrophilic polyHEMA swollen with water. The electron density of the first layer was fixed to that of bulk polySB, and that of the second layer was varied between 0.396 (HEMA) and 0.334 Å^{-3} (H_2O). The thickness of the first (d_1) and the second layers (d_2), the roughness for the air/first layer (σ_1), the first layer/second layer (σ_{12}), and the second layer/water (σ_2) interfaces were adjustable parameters, where the roughness is introduced as a standard deviation of Gaussian distribution function to take into account the density profile at the interface.

Atomic Force Microscopy (AFM). AFM measurements were performed by SPI3800 probe station and SPA300 unit system of the scanning probe microscopy system (SPI3800 series; Seiko Instruments, Tokyo, Japan). The cantilever was made of silicon (Olympus, Tokyo, Japan), and its spring constant was 20 N/m. The measurements were performed in dynamic force mode (noncontact mode). For sample preparation, a chloroform solution of the polymer was spread at the water surface in a LB trough to form a polymer film. Then the polymer film was deposited on a micro slide glass (IWAKI, Japan) at a designated surface pressure, and the film was dried in a desiccator with silica gel for at least 3 days.

Scheme 1

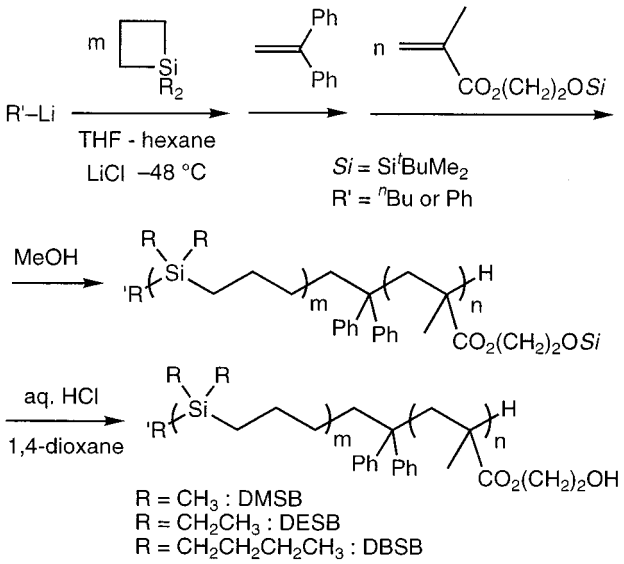

Results and Discussion

Synthesis and Characterization of Poly(SB-*b*-HEMA)s. Amphiphilic block copolymers composed of polyHEMA and polyDMSB, polyDESB, or polyDBSB were synthesized by addition of Si-HEMA to the corresponding living polySB capped with 1,1-diphenylethylene and successive deprotection of silyl group in poly(Si-HEMA) segment (Scheme 1). We prepared three block copolymers with different compositions of polySB and polyHEMA (ca. 10:40, 10:20, 20:20) as samples by just changing the monomer/initiator ratio in polymerization. The GPC charts for the representative copolymers before hydrolysis of silyl protecting groups are given in Figure 1. The GPC charts clearly shifted to a higher molecular weight region by addition of Si-HEMA monomer with a narrow molecular weight distribution in all cases, indicating the formation of the block copolymers. We determined the number-averaged polymerization degrees of polySB and polyHEMA segments by ^{1}H NMR measurement and the molecular weight distribution of the block copolymer by GPC using polystyrene as calibration standards. These values are listed in Table 1. These copolymers were soluble in methanol, though polySB is insoluble in methanol, because they have relatively long polyHEMA segments, which are soluble in methanol. However, they are insoluble in water since neither polySB nor polyHEMA is soluble in water.

Thermal Behavior of Bulk Polymers. At room temperature, DMSB homopolymer is in a crystalline state, while polyDESB and polyDBSB are in a melt state. To examine the thermal properties of polySBs in detail, DSC measurements for the homopolymers were performed. An endothermic peak due to the melt transition was observed around 29 °C for polyDMSB (Figure 2), while the other homopolymers did not show such transitions from −100 to 100 °C. No glass transition was observed for all samples, indicating the high flexibility of polySB chains. The endothermic peak due to the melt transition of polyDMSB segment was also observed around room temperature even in the block copolymer. Figure 3 shows the DSC second heating scan of poly(DMSB-*b*-HEMA) (*m*:*n* = 19:21). The melt transition was observed at 22 °C, though the peak was obscure compared with that of the homopolymer. This crystal-line−melt transition may be one of the most important features of poly(DMSB-*b*-HEMA).

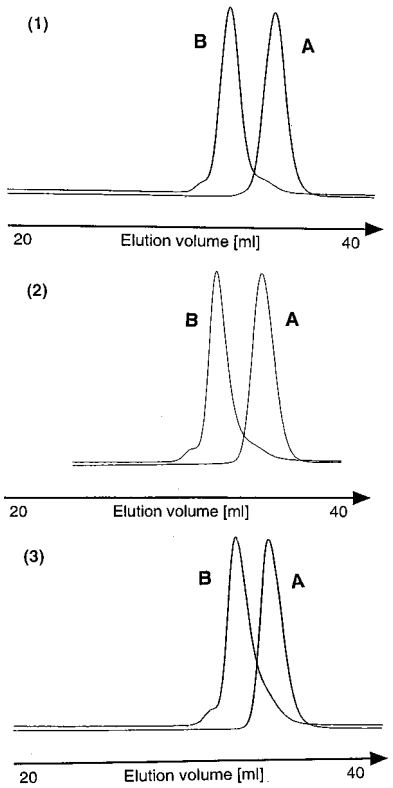

Figure 1. GPC charts for poly(SB-*b*-Si-HEMA). (1) (A) polyDMSB (*m* = 19), (B) poly(DMSB-*b*-Si-HEMA) (*m*:*n* = 19:21). (2) (A) polyDESB (*m* = 26), (B) poly(DESB-*b*-Si-HEMA) (*m*:*n* = 26:24). (3) (A) polyDBSB (*m* = 18), (B) poly(DBSB-*b*-Si-HEMA) (*m*:*n* = 18:21).

Table 1. Characterization of Poly(SB-*b*-HEMA)

polymer	m^a	n^a	$M_n{}^a$	$M_w/M_n{}^b$
poly(DMSB-*b*-HEMA)	13	38	6500	1.25
	10	23	4200	1.16
	19	21	4800	1.13
poly(DESB-*b*-HEMA)	13	37	6700	1.28
	12	22	4700	1.20
	26	24	6700	1.20
poly(DBSB-*b*-HEMA)	11	35	6700	1.21
	10	20	4700	1.15
	18	21	6300	1.18

[a] Determined by ^{1}H NMR. [b] Determined by GPC using polystyrene as a standard.

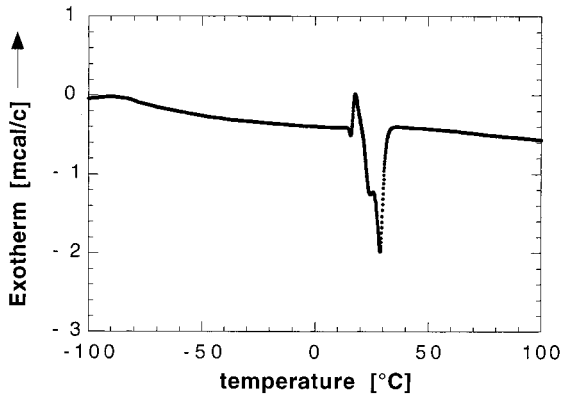

Figure 2. DCS curve for the second heating scan of polyDMSB (*m* = 19) at the rate of 10 °C/min.

Association Behavior of Poly(SB-*b*-HEMA)s in Methanol. The association behavior of poly(SB-*b*-

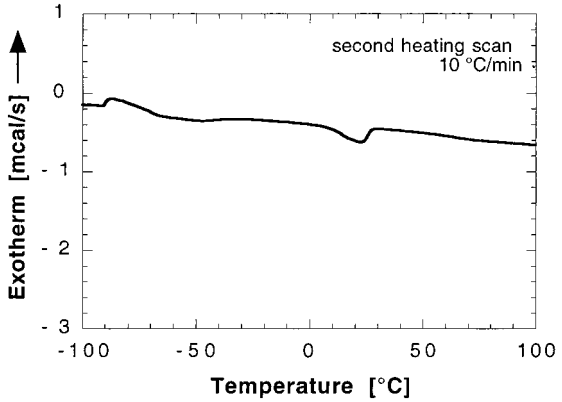

Figure 3. DCS curve for the second heating scan of poly(DMSB-*b*-HEMA) (*m*:*n* = 19:21) at the rate of 10 °C/min.

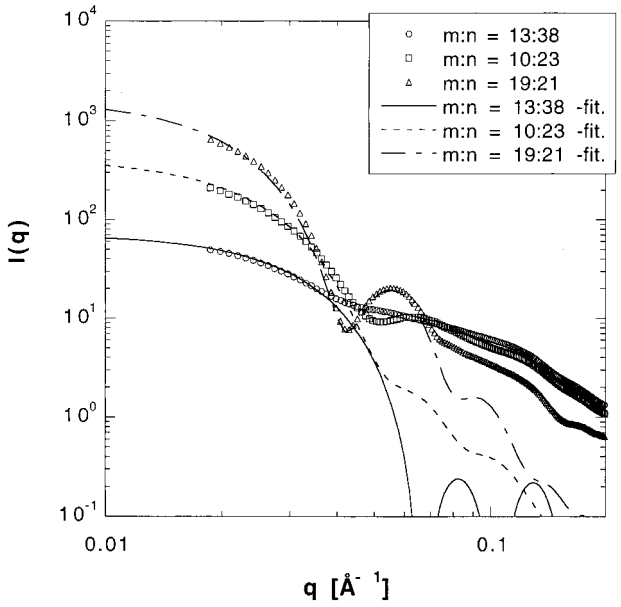

Figure 4. SAXS profiles for 1 wt % methanol solution of poly(DMSB-*b*-HEMA) *m*:*n* = (○) 13:38, (□) 10:23, and (△) 19:21. The solid, dotted, and broken lines are the best fitting curves calculated from core−shell sphere models.

HEMA)s in methanol was examined by SAXS. Figure 4 shows the SAXS profiles for poly(DMSB-*b*-HEMA) 1 wt % methanol solutions at 25 °C. Three polymers with different block ratios (*m*:*n*) were examined. Strong scattering was observed at the small angle regions in all cases, indicating the formation of micelles in solutions. In addition, a secondary maximum at $q \approx 0.06$ Å^{-1}, implying a core−shell structure and a relatively narrow size distribution of the micelle in the case of copolymers of (*m*:*n* = 19:21 and *m*:*n* = 10:23). To analyze the SAXS data, we assumed a core−shell spherical micelle model, whose core consisted of polyDMSB and shell consisted of polyHEMA swollen by methanol, and calculated the theoretical scattering curve for the model. The calculated curve shown in Figure 4 fitted to the experimental data well especially at the small-angle regions. The deviation at a larger angle region is due to the effect of blob scattering; the scattering at larger angles is affected by individual fluctuation of polymer chains in the shell,[22,23] which is not taken account in the present model. Also, the large deviation seen in the profile of poly(DMSB-*b*-HEMA) (*m*:*n* = 13:38), which has the lowest content of hydrophobic segment, may be caused by the scattering from

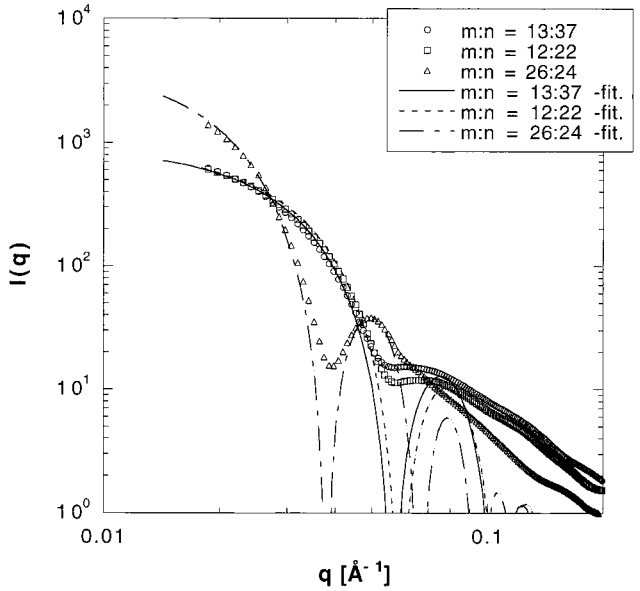

Figure 5. SAXS profiles for 1 wt % methanol solution of poly(DESB-*b*-HEMA) *m*:*n* = (○) 13:37, (□) 12:22, and (△) 26:24 at 25 °C. The solid, dotted, and broken lines are the best fitting curves calculated from core−shell sphere models.

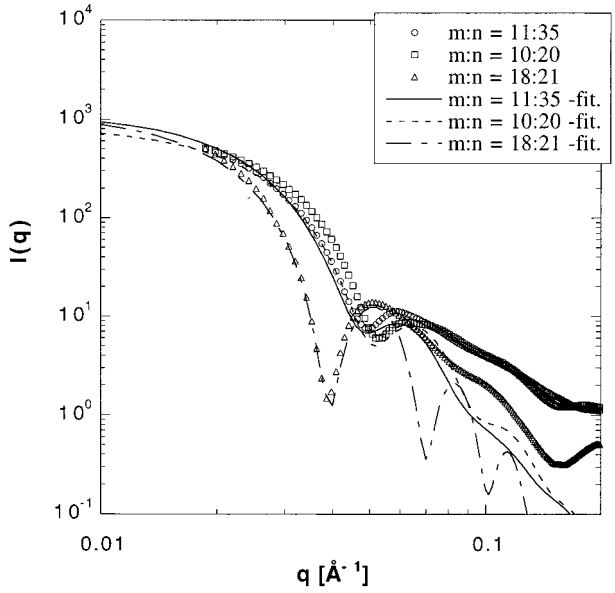

Figure 6. SAXS profiles for 1 wt % methanol solution of poly(DBSB-*b*-HEMA) *m*:*n* = (○) 11:35, (□) 10:20, and (△) 18:21. The solid, dotted, and broken lines are the best fitting curves calculated from core−shell sphere models.

a unimer that is a molecularly dissolved polymer molecule. The SAXS profiles obtained from poly(DESB-*b*-HEMA) and poly(DBSB-*b*-HEMA) 1 wt % methanol solutions at 25 °C are given in Figures 5 and 6. A strong scattering was also observed in these cases, and the theoretical curves for the analogous core−shell sphere model well reproduced the experimental data. The fitting results for all the samples are summarized in Table 2. From Table 2, a qualitative relationship between micellar structure and polymer composition or substituent on silicon atoms can be found. The radius of core and the aggregation number increased as the content of polySB in the block copolymer chain increased, and they also increased with increasing number of carbon atoms in the substituent at silicon atom. We suppose that increases in aggregation number is due

Table 2. SAXS Fitting Parameters for Micelles Formed by Poly(SB-*b*-HEMA) in Methanol

polymer	*m*:*n*	R_c[a]	R_s[b]	ϕ_{Sol}[c]	σ_{R_s}/R_s[d]	N_{agg}[e]
poly(DMSB-*b*-HEMA)	13:38	14	70	0.98		6
	10:23	23	80	0.95	0.19	26
	19:21	52	96	0.82	0.15	155
poly(DESB-*b*-HEMA)	13:37	28	78	0.93	0.11	27
	12:22	33	76	0.91	0.12	47
	26:24	64	105	0.85	0.12	164
poly(DBSB-*b*-HEMA)	11:35	42	86	0.79	0.18	81
	10:20	46	79	0.76	0.16	112
	18:21	70	109	0.80	0.05	216

[a] The radius of the core. [b] The radius of the overall micelle. [c] The volume fraction of the solvent in the shell. [d] The polydispersity of the overall micellar size. [e] The aggregation number.

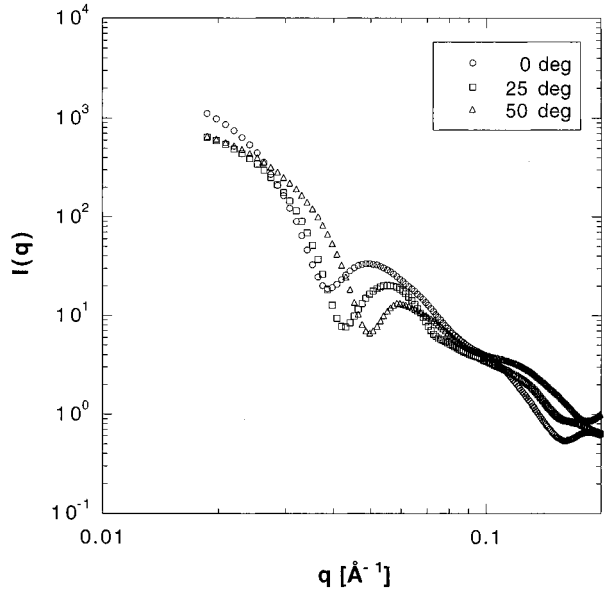

Figure 7. SAXS profiles for 1 wt % methanol solution of poly(DMSB-*b*-HEMA) (*m*:*n* = 19:21) at (○) 50, (□) 25, and (△) 0 °C.

to the increase of steric bulkiness of hydrophobic polySB segment relative to the hydrophilic polyHEMA segment. More copolymer molecules must be needed in order to cover the surface of the hydrophobic core effectively with hydrophilic chains.

Since bulk poly(DMSB-*b*-HEMA) (*m*:*n* = 19:21) exhibited morphology transition as confirmed by DSC measurement, it was expected that its association behavior in solution might also be influenced by the solution temperature. In fact, the methanol containing 1 wt % poly(DMSB-*b*-HEMA) (*m*:*n* = 19:21) is a transparent solution above room temperature, while it is a turbid dispersion below room temperature. Furthermore, the transition is completely reversible. To examine the temperature dependence of the association behavior, we carried out SAXS measurements of 1 wt % block copolymers in methanol at various temperatures. The SAXS profiles for the solution of poly(DMSB-*b*-HEMA) at 0, 25, and 50 °C are shown in Figure 7. A marked difference was found in the profiles of poly(DMSB-*b*-HEMA), while the same scattering patterns were observed in poly(DESB-*b*-HEMA) and poly(DBSB-*b*-HEMA). The initial slope of the profile around $0.02 < q < 0.04$ Å^{-1} became steeper, and the second peak position around $q = 0.06$ Å^{-1} shifted to smaller angle regions with the lowering of temperature, indicating a formation of the larger aggregates at the lower temperature. However, it is difficult to analyze the micelle

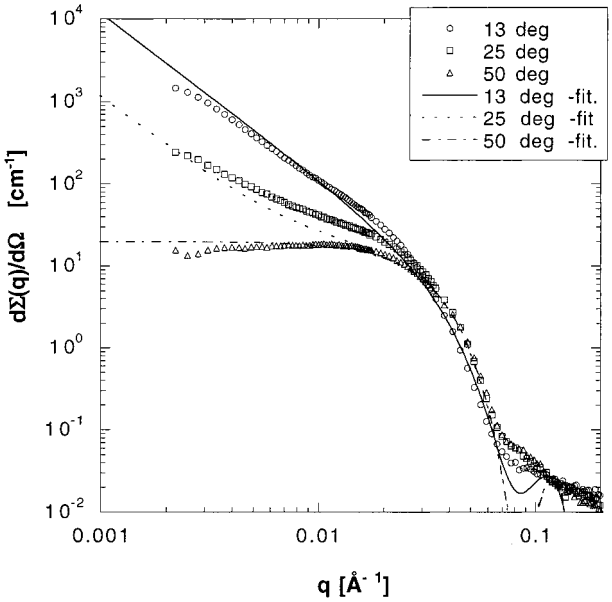

Figure 8. SANS profiles for 1 wt % methanol solution of poly(DMSB-*b*-HEMA) (*m*:*n* = 19:21) at (△) 50, (□) 25, and (○) 13 °C. The solid, dotted, and broken lines are the best fitting curves calculated from coexistence model of spherical and disklike micelles.

structure only by SAXS data because of the lack of the smaller angle information.

To examine in detail the temperature dependence of the micelle structure formed by poly(DMSB-*b*-HEMA), we performed SANS measurement at three different temperatures, which gave us more information in smaller angle regions. Figure 8 shows the SANS profiles obtained from 1 wt % poly(DMSB-*b*-HEMA) solution at 13, 25, and 50 °C. The secondary maximum near $q = 0.06$ Å^{-1} was not observed in the SANS curve. The difference of the scattering profiles between SAXS and SANS supported the assumption that micelles consist of a core−shell structure. As was mentioned in the Experimental Section, the electron density of the shell is higher than that of the core or the solvent, which gives the secondary maximum in the SAXS profile. However, since the scattering length density contrast between the core and the shell is considerably low compared with that between the shell and the solvent, the SANS profile does not have the secondary maximum. The three SANS profiles in Figure 8 showed marked differences by changing the temperature. The profile obtained at 50 °C showed a typical profile of sphere particle (that region at smaller angle), indicating the formation of spherical micelles. In the contrast, the profile obtained at 13 °C is approximately proportional to q^{-2} in the smaller angle regions at $q < 0.01$ Å^{-1}. The profile strongly suggests the formation of disklike micelles, since the scattering intensity of infinitely large and infinitely thin disk is proportional to q^{-2}.[24] This scattering behavior could not be observed in the SAXS profile in Figure 7, because it was beyond the measurable q range of SAXS, which does not cover such a smaller angle region. We calculated theoretical curves for core−shell disk micelle and fitted them to the experimental data. The calculated curve could very well reproduce the experimental data with reasonable structural parameters. The profile taken at 25 °C was the intermediate between profiles at 50 and 13 °C. It is presumably because core−shell sphere micelles and core−shell disk micelles coexist in the solution at this

Table 3. Fitting Parameters for SANS Data of Poly(DMSB-*b*-HEMA) (*m*:*n* = 19:21) Micelles in Methanol Solutions Using Coexistence Model of Sphere and Disklike Micelles

temp [°C]	shape	ϕ_{disk}[a]	R_c[b] [Å]	R_s[c] [Å]	ϕ_{sol}[d]	N_{agg}[e]
13	disk	1	L_c[f] = 40	L_s[g] = 120	0.52	
25	disk	0.10	L_c = 40	L_s = 120	0.52	
	sphere		53	92	0.78	160
50	sphere		53	92	0.78	160

[a] The volume fraction of disklike micelle. [b] The radius of the core. [c] The radius of the whole micelle. [d] The volume fraction of solvent in the shell. [e] The aggregation number. [f] The thickness of the inner layer. [g] The thickness of the outer layer.

particular temperature. Then we assumed a sphere−disk coexistence model, where both micelles were present in the solution with the volume fraction of ϕ_{sphere} and ϕ_{disk}, and calculated the SANS curves according to eq 15. Here, the structure of the spherical micelles involved in the solution at 25 °C was assumed to be the same as that at 50 °C. Similarly, the structure of disklike micelles at 25 °C was thought to be the same as that at 13 °C. The fitting results are listed in Table 3.

We consider that the sphere−disk transition was driven by melting−crystallization of polyDMSB segment. We have reported the analogous sphere−disk transition of polymer micelles formed by poly(2-hydroxyethyl vinyl ether) having octadecyl group at the chain end, which is caused by melting−crystallization transition of the octadecyl group.[25] To the best of our knowledge, however, the structural transition observed here is a very rare example of block copolymer micelles. The micelles of so-called Pluronic polymers (e.g., PEO−PPO−PEO, etc.) are well-known to be temperature-sensitive micelles: they become larger, and the solution tends to be turbid.[4c,g] This phenomenon is explained by the dehydration of EO segments with increasing temperature. In the present case, a clearer and drastic morphology change (sphere−disk) is induced by lowering temperature, and its origin is the crystallization of the hydrophobic segment.[26] It is interesting to pay attention to the present system as a novel temperature responsible system.

Thin-Layer Formation by Poly(SB-*b*-HEMA)s at the Water Surface. Since polyHEMA is not soluble in water but has enough affinity to water, the poly(SB-*b*-HEMA) is expected to form a stable thin layer on the water surface. Then, we spread poly(SB-*b*-HEMA) chloroform solutions on the water surface and examined the behavior of the copolymer. Three block copolymers, poly(DMSB-*b*-HEMA), poly(DESB-*b*-HEMA), and poly(DBSB-*b*-HEMA), with almost the same polymerization degrees of polySB and polyHEMA segments were used as samples. The $\pi-A$ isotherms of the copolymer layers spread on the water surface are shown in Figure 9. By compressing the water surface, the surface pressure gradually increased and finally reached over 40 mN/m, indicating the formation of stable polymer layers in all cases. All the isotherms exhibit two regions. One is a low surface pressure region less than 20 mN/m where the surface pressure gradually increased with the compression, and the other is a high surface pressure region more than 20 mN/m where the surface pressure abruptly increased with the compression. It is supposed that, in the low surface pressure regions, the polymers are molecularly distributed on the water surface in random and the contact of the polymer chains by compression increases the surface pressure gradually.

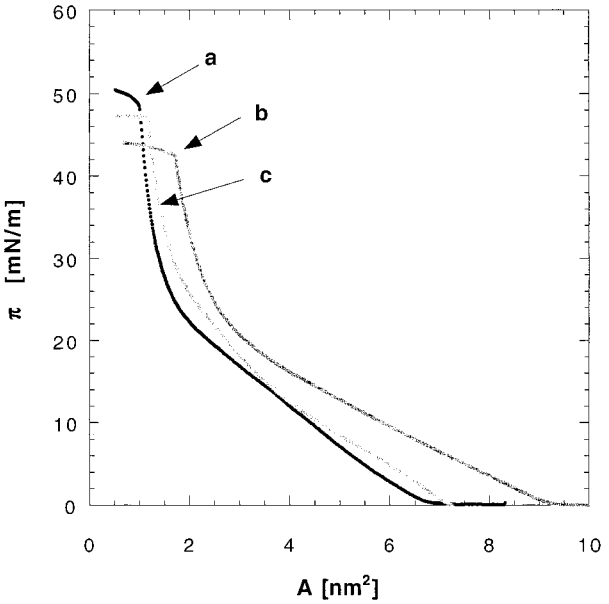

Figure 9. $\pi-A$ isotherms for (a) poly(DMSB-*b*-HEHA) (*m*:*n* = 19:21), (b) poly(DESB-*b*-HEMA) (*m*:*n* = 26:24), and (c) poly(DBSB-*b*-HEMA) (18:21) spread on the water surface at 25 °C.

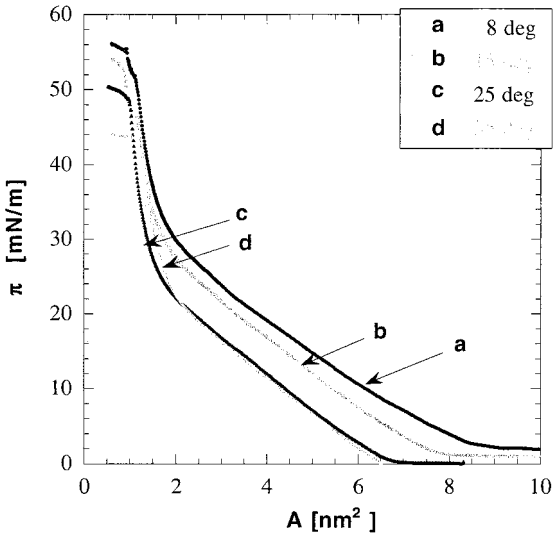

Figure 10. $\pi-A$ isotherms for poly(DMSB-*b*-HEMA) (19:21) spread on the water surface at (a) 8, (b) 15, (c) 25, and (d) 35 °C.

In the higher surface pressure region, the polymer molecules are already fully contacted in a two-dimensional way, and well-structured two layered monolayer of the polymers are formed by further compression with increasing layer thickness.

Since poly(SB-*b*-HEMA) showed strong temperature dependence on micelle formation as previously discussed, it is fair to expect that the $\pi-A$ isotherm of this block copolymer monolyaer has a unique temperature dependence. Figure 10 shows the $\pi-A$ isotherm at various temperatures. The surface pressure where the film collapses increased with lowered temperature, indicating that a stiffer and tougher polymer film was formed at lower temperature. Isotherms taken at 25 and 35 °C coincided well with each other but were quite different from those obtained at 8 and 15 °C. The area per molecule at a certain surface pressure on the isotherms increased as the temperature decreased. Such temperature dependence of the $\pi-A$ isotherm was not

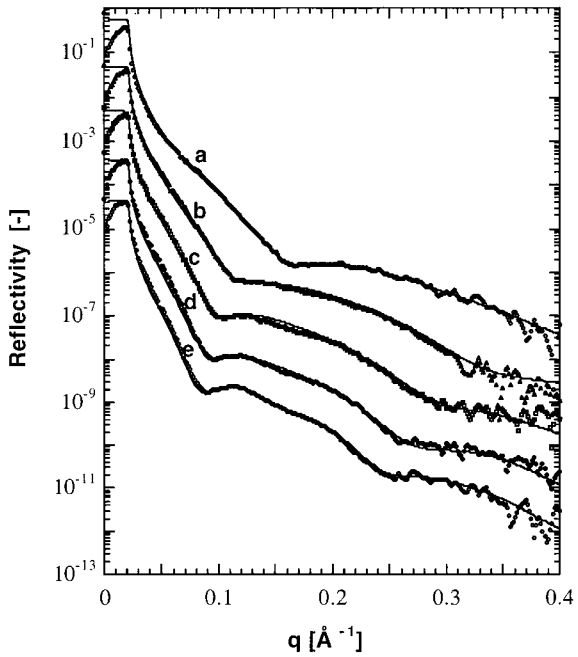

Figure 11. XR profiles for poly(DMSB-*b*-HEMA) monolayer spread on the water surface at (a) 20, (b) 25, (c) 30, (d) 35, and (e) 40 mN/m. The solid lines are the best fitting curves calculated by assuming two-layer models.

Table 4. XR Fitting Parameters for Monolayer of Poly(DMSB-*b*-HEMA) (*m*:*n* = 19:21)

π^a [mN/m]	A^b [Å^2]	$d_1{}^c$ [Å]	$d_2{}^d$ [Å]	$\sigma_1{}^e$ [Å]	$\sigma_{12}{}^f$ [Å]	$\sigma_2{}^g$ [Å]
20	180	19	19	3.4	3.6	6.4
25	120	27	28	3.5	3.6	13
30	110	32	35	4.0	3.6	13
35	70	35	37	4.0	3.6	12
40	60	37	40	4.0	3.6	7.5

[a] Surface pressure. [b] Area per molecule. [c] Thickness of polyDMSB layer. [d] Thickness of polyHEMA layer. [e] Roughness of polyDMSB surface. [f] Roughness of polyDMSB−polyHEMA interface. [g] Roughness of polyHEMA−water interface.

observed in poly(DBSB-*b*-HEMA) and poly(DESB-*b*-HEMA) in the same temperature range. Hence, the poly(DMSB-*b*-HEMA) monolayer on water can attract attention as a temperature-sensitive polymer monolayer near ambient temperature as well as its micelle in methanol, although further studies are necessary to clarify the mechanism of this phenomenon in detail.

To examine the film nanostructure in detail, XR measurements were performed of the block copolymer monolayers spread on the water surface at 28 °C, which is just above the melting temperature of polyDMSB segment. The surface pressure was 20, 25, 30, 35, or 40 mN/m. Figure 11 shows the XR profiles for poly(DMSB-*b*-HEMA). Kiessig fringes[27] were clearly observed up to the third order, indicating the formation of copolymer monolayer with a uniform thickness and smooth interfaces. The shift of the fringes toward the smaller angle region with the compression of the layer indicated the increase of the layer thickness, which is similar to the reported results of poly(DESB-*b*-HEMA).[14] To analyze the XR data, we applied the two-layer model in which the upper layer is composed of hydrophilic polySB and the lower layer is composed of polyHEMA swollen with water. The theoretical profile for the model fitted well to the experimental data as shown in Figure 11. The fitting parameters are summarized in Table 4. It was confirmed that the copolymer monolayer, whose upper side consists of polyDMSB and lower side consists of hydrated polyHEMA, was formed with very low roughness all the time. It is worth emphasizing here that the extremely flat and smooth surface and interface for the monolayers of these block copolymers has never been observed: to the authors' knowledge, clearness of the Kiessig fringes in Figures 11 and 12 is outstanding as the one for polymer monolayer on water (on solid substrate). This is due to the very flexible nature of the Si-containing segments and also is one of the advantages of these block copolymer systems.

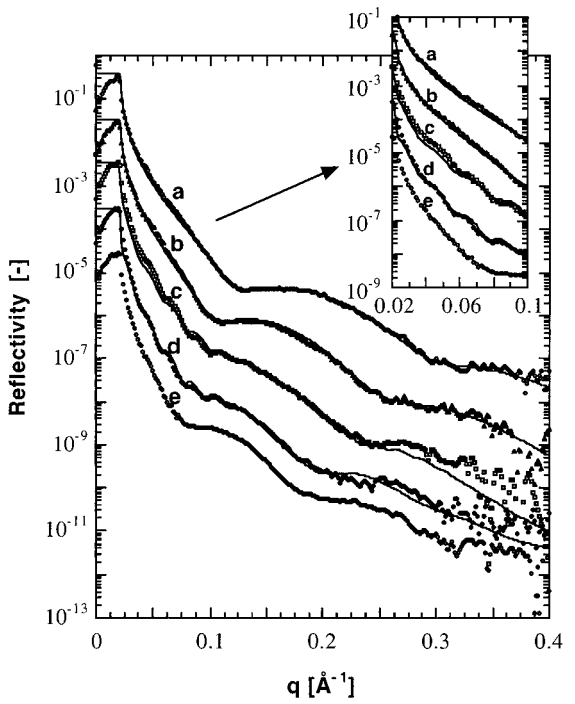

Figure 12. XR profiles for poly(DBSB-*b*-HEMA) spread on the water surface at (a) 20, (b) 25, (c) 30, (d) 35, and (e) 40 mN/m. The solid lines are the best fitting curves calculated from the two-layer model (a, b) or three-layer models (c, d).

Figure 12 depicts the XR profiles for poly(DBSB-*b*-HEMA) on the water surface. Clear Kiessig fringes were observed, and the fringes shifted to smaller angle region with the increase of surface pressure as in the case of poly(DMSB-*b*-HEMA). In the profiles taken at 30 and 35 mN/m, however, another series of fringes with shorter frequency were observed in the q range from 0.02 to 0.10 Å^{-1} as shown in the inset of Figure 12. These fringes were not observed in the profiles at 20, 25, and 40 mN/m. This indicates the existence of other relatively thick layers than the usual thin monolayer at the high surface pressure. For the "normal" profile such as for low surface pressure, two-layer model consisting of water/hydrophobic SB layer/hydrophilic HEMA layer/water was applied for XR profile analysis. The results are shown in Table 5. The thickness of the SB layer changed from 30 to 36 Å with the increase of the surface pressure from 20 to 25 mN/m. As was reported previously, the continuous increase of SB layer thickness indicates the flexibility of SB segments. The thickness of HEMA layer changed from 14 to 17 Å. The rather small thickness of this layer is supported by the insoluble nature of HEMA segment to water: the HEMA chains are located and spread almost two-dimensionally near the interface between SB layer and water subphase.

Table 5. XR Fitting Parameters for Poly(DBSB-*b*-HEMA) (*m*:*n* = 19:21) Spread on the Water Surface

		layer 1		layer 2	
π^a [mN/m]	A^b [Å^2]	$\phi_{\text{layer 1}}{}^c$	$d_1{}^d$[Å]	$d_{\text{SB}}{}^e$[Å]	$d_{\text{HEMA}}{}^f$[Å]
20	129			30	14
25	107			36	17
30	91	0.40	280	41	18
35	51	0.65	300	48	20

[a] Surface pressure. [b] Area per molecule. [c] Area fraction of layer 1. [d] Thickness of layer 1. [e] Thickness of polySB layer in layer 2. [f] Thickness of polyHEMA layer in layer 2.

For the "abnormal" profiles under 30 and 35 mN/m conditions, the two-layer model clearly breaks down; hence, we applied a new model that was a thicker one-layer and thinner two-layer coexisting model. In this model, the multimolecular one-layer composed of a homogeneous mixture of polySB and polyHEMA segments covered a part of the water surface, and the rest was covered with SB-HEMA monolayer. Now we call the former layer layer 1 and the latter one layer 2. The area fraction of layer 1 was described as $\phi_{\text{layer 1}}$. Including $\phi_{\text{layer 1}}$ and d_1 (thickness of layer 1) as fitting parameters, we found the best model to reproduce both the "slow fringe" and "fast fringe". In this model, we assumed an island model which was also used for the lamellar structure of block copolymer film.[28] For d_{SB} and d_{HEMA}, a continuous increase by compression was observed as is shown in Table 5. For d_1, the thickness was almost 300 Å with a half-island/half-sea structure, and it slightly increased with increasing surface pressure. The fraction $\phi_{\text{layer 1}}$ also increased with increasing surface pressure. We cannot interpret this rather large thickness of the layer 1 at this stage, but it can be said that this is a flat island structure formed by compression of flexible block copolymer.

Structure of Poly(DBSB-*b*-HEMA) Film Deposited on a Glass Plate. To clarify the special characteristics of poly(DBSB-*b*-HEMA) thin layer as described above, AFM observation was applied to the film deposited on a glass plate. AFM images obtained are shown in Figure 13a−c. These surface images of the copolymer film deposited at different surface pressure looks largely different. A marked smooth surface was observed in Figure 13a (for 20 mN/m). At 30 mN/m, many small aggregates arranged evenly on a copolymer film, whose diameter was ca. 30 nm, were observed in Figure 13b. In Figure 13c (for 35 mN/m), a relatively rough surface was observed, which was probably due to the growth or fusion of small aggregates seen in Figure 13b. The size of the assembled aggregates was roughly 100 Å in diameter. The flat surface at 20 mN/m by AFM observation is consistent with the XR result mentioned above. The similar small two-dimensional aggregates as those for 30 mN/m by AFM was also observed for a poly(α-methylstyrene-*b*-quaternized-4-vinylpyridine) monolayer on water,[29] and enhancement of aggregate structure by a depositing and/or drying process was confirmed by comparison of in-situ XR and AFM measurements. Taking this factor into mind, the present XR and AFM results for 30 mN/m are not inconsistent. For 35 mN, the XR profile suggested an island−sea structure as was shown in Figure 12. This nature is supported by Figure 13c showing also an island−sea, although the structure itself is not quantitatively the same for on water and on glass substrate.

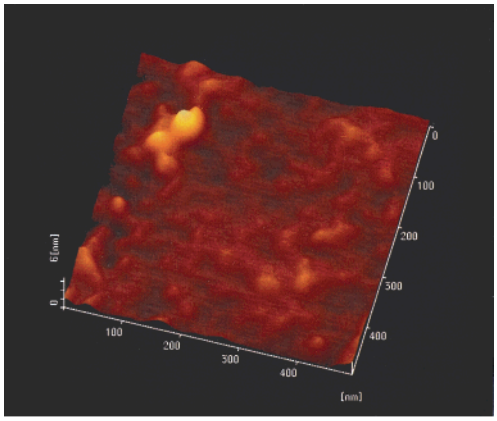

Figure 13. AFM images of poly(DBSB-*b*-HEMA) films deposited on the glass plate at (a) 20, (b) 30, and (c) 35 mN/m.

Conclusions

Amphiphilic block copolymers, poly(SB-*b*-HEMA), having various alkyl groups on silicon atoms, were synthesized with controlling the chain lengths of both segments by a living anionic polymerization of 1,1-dialkylsilacyclobutane and silyl-protected 2-hydroxyethyl methacrylate. It was confirmed that the poly(SB-*b*-HEMA)s formed micelles in methanol and that the aggregation number of the micelles increased with the increase of the polySB content or number of carbon

atoms in the alkyl substituents. It was also found that poly(DMSB-*b*-HEMA) exhibits a strong temperature dependence on the association behavior, i.e., sphere-to-disk transition of the micelle, with decreasing temperature, which may be caused by crystallization of hydrophobic polyDMSB segment. To confirm the disklike micelle formation, direct microscopic observations such as transmission electron microscopy (TEM) and AFM of deposited micelle solutions may be helpful,[3a,c,d,30] which we are now planing to apply to our system.

Poly(SB-*b*-HEMA) with almost the same polymerization degrees of polySB and polyHEMA segments formed stable spread monolayers on the water surface. Very smooth surface and interfaces were confirmed by in-situ XR analysis. For poly(DBSB-*b*-HEMA) on the water surface at higher surface pressure, however, formation of an island−sea structure was suggested by in-situ XR analysis, which was also supported by AFM observation for deposited film on a glass substrate.

As we have demonstrated here, amphiphilic block copolymers having polySBs as hydrophobic segments are thought to be very attracting and useful samples for detailed investigation of self-organization of polymeric amphiphiles both in solution and at interfaces.

Acknowledgment. This work was supported by a Grant-in-aid from the Ministry of Education, Culture, Sports, Science and Technology (No. A09305062). We are deeply grateful to Dr. M. Nagao for his kind support of SANS measurements at Tokai, which was adopted as Proposal 00.060.

References and Notes

(1) (a) Alexandridis, P., Lindman, B., Eds.; *Amphiphilic Block Copolymers*; Elsevier: Amsterdam, 2000. (b) Bock, J.; Varadaraj, R.; Schultz, D. N.; Maurer, J. J. In *Macromolecular Complexes in Chemistry and Biology. Solution Properties of Hydrophobically Associating Water-Soluble Polymers*; Dubin, P., Bock, J., Davis, R., Schulz, D. N., Thies, C., Eds.; Springer-Verlag: Berlin, 1994; p 33. (c) Tuzar, Z.; Kratochvil, P. In *Surface and Colloid Science*; Matijevic, E., Ed.; Plenum Press: New York, 1993; Vol. 15; Chapter 1, pp 1−83. (d) Piirma, I. *Polymeric Surfactants;* Surfactant Science Series Vol. 42; Marcel Dekker: New York, 1992. (e) Zhang, Y. X.; Da, H. A.; Hogen-Esch, T. E.; Bulter, G. B. In *Water Soluble Polymers: Synthesis, Solution Properties, and Application*; Shalaby, S. W., McCormik, C. L., Buller, G. B., Eds.; ACS Symposium Series 467; American Chemical Society: Washington, DC, 1991; p 159.

(2) (a) Halperin, A.; Tirrell, M.; Lodge, T. P. *Adv. Polym. Sci.* **1992**, *100*, 31. (b) Moffitt, M.; Khougaz, K.; Eisenberg, A. *Acc. Chem. Res.* **1996**, *29*, 95. (c) Chu, B. *Langmuir* **1995**, *11*, 414. (d) Hawmleg, I. W., Ed.; *The Physics of Block Copolymers*; Oxford Science: Oxford, 1998.

(3) For micelle formation of diblock copolymers, see: (a) Schuch, H.; Klingler, J.; Rossmanith, P.; Frechen, T.; Gerst, M.; Feldthusen, J.; Müller, A. H. E. *Macromolecules* **2000**, *33*, 1734. (b) Nakano, M.; Matsuoka, H.; Yamaoka, H.; Poppe, A.; Richter, D. *Macromolecules* **1999**, *32*, 697. (c) Yu, Y.; Zhang, L.; Eisenberg, A. *Macromolecules* **1998**, *31*, 1144. (d) Yu, K.; Eisenberg, A. *Macromolecules* **1998**, *31*, 3509. (e) Mortensen, K.; Brown, W.; Almdal, K.; Alami, E.; Jada; A. *Langmuir* **1997**, *13*, 3635. (f) Topp, M. D. C.; Dijkstra, P. J.; Talsma, H.; Feijen, J. *Macromolecules* **1997**, *30*, 8518. (e) Poppe, A.; Willner, L.; Allgaier, J.; Stellbrink, J.; Richter, D. *Macromolecules* **1997**, *30*, 7462. (f) Jada, A.; Hurtrez, G.; Siffert, B.; Riess, G. *Macromol. Chem. Phys.* **1996**, *197*, 3697. (g) Yu, K.; Eisenberg, A. *Macromolecules* **1996**, *29*, 6359. (h) Hickl, P.; Jada, A. *Macromolecules* **1996**, *29*, 4006. (i) Zhang, L.; Barlow, R. J.; Eisenberg, A. *Macromolecules* **1995**, *28*, 6055. (j) Zhang, L.; Eisenberg, A. *Science* **1995**, *268*, 1728. (k) Qin, A.; Tian, M.; Ramireddy, C.; Webber, S. E.; Munk, P.; Tuzar, Z. *Macromolecules* **1994**, *27*, 120. (l) Gao, Z.; Varshney, S. K.; Wong, S.; Eisenberg, A. *Macromolecules* **1994**, *27*, 7923. (m) Xu, R.; Winnik, M. A.; Riess, G.; Chu, B.; Croucher, M. D. *Macromolecules* **1992**, *25*, 644.

(4) For micelle formation of amphiphilic triblock copolymers, see: (a) Mortensen, K.; Talmon, Y.; Gao, B.; Kops, J. *Macromolecules* **1997**, *30*, 6764. (b) Wu, G.; Chu, B.; Schneider, D. K. *J. Phys. Chem.* **1995**, *99*, 5094. (c) Glatter, O.; Scherf, G.; Schillén, K.; Brown, W. *Macromolecules* **1994**, *27*, 6046. (d) Mortensen, K.; Brown, W.; Jørgensen, E. *Macromolecules* **1994**, *27*, 5654. (e) Schillén, K.; Brown, W.; Johnsen, R. M. *Macromolecules* **1994**, *27*, 4825. (f) Zhou, Z.; Chu, B. *Macromolecules* **1994**, *27*, 2025. (g) Mortensen, K.; Pendersen, J. S. *Macromolecules* **1993**, *26*, 805.

(5) For synthesis and properties of silicon-containing amphiphilic block copolymers, see: (a) Báñez, M. V.; Robinson, K. L.; Armes, S. P. *Macromolecules* **2000**, *33*, 451. (b) Sanji, T.; Nakatsuka, Y.; Ohnishi, S.; Sakurai, H. *Macromolecules* **2000**, *33*, 8524. (c) Sanji, T.; Kitayama, F.; Sakurai, H. *Macromolecules* **1999**, *32*, 5718. (d) Resendes, R.; Massey, J.; Dorn, H.; Winnik, M. A.; Manners, I. *Macromolecules* **2000**, *33*, 8.

(6) Dizhoor, A. M.; Ray, S.; Kumar, S.; Niemi, G.; Spencer, M.; Brolley, D.; Walsh, K. A.; Philipov, W. P.; Hurley, J. B.; Stryer, L. *Science* **1991**, *251*, 915.

(7) (a) Fauré, M. C.; Bassereau, P.; Lee, L. T.; Menelle, A.; Lheveder, C. *Macromolecules* **1999**, *32*, 8538. (b) Kago, K.; Matsuoka, H.; Yoshitome, R.; Mouri, E.; Yamaoka, H. *Langmuir* **1999**, *15*, 4295. (c) An, S. W.; Thomas, R. K.; Baines, F. L.; Billingham, N. C.; Armes, S. P.; Penfold, J. *Macromolecules* **1998**, *31*, 7877. (d) An, S. W.; Thomas, R. K.; Baines, F. L.; Billingham, N. C.; Armes, S. P.; Penfold, J. *J. Phys. Chem. B* **1998**, *102*, 5120. (e) An, S. W.; Su, T. J.; Thomas, R. K.; Baines, F. L.; Billingham, N. C.; Armes, S. P.; Penfold, J. *J. Phys. Chem. B* **1998**, *102*, 387. (f) Gonçalves da Silva, A. M.; Simões Gamboa, A. L.; Martinho, J. M. G. *Langmuir* **1998**, *14*, 5327. (g) Rother, G.; Findenegg, G. H. *Colloid Polym. Sci.* **1998**, *276*, 496. (h) Richards, R. W.; Rochford, B. R.; Webster, J. R. P. *Polymer* **1997**, *38*, 1169. (i) Ahrens, H.; Förster, S.; Helm, C. A. *Macromolecules* **1997**, *30*, 8447. (j) Gonçalves da Silva, A. M.; Filipe, E. J. M.; d'Oliveira, J. M. R.; Marthinho, J. M. G. *Langmuir* **1996**, *12*, 6547. (k) Li, Z.; Zhao, W.; Quinn, J.; Rafailovich, M. H.; Sokolov, J.; Lennox, R. B.; Eisenberg, A.; Wu, X. Z.; Kim, W.; Sinha, S. K.; Tolan, M. *Langmuir* **1995**, *11*, 4785. (l) Bijsterbosch, H. D.; de Haan, V. O.; de Graaf, A. W.; Mellema, M.; Leermakers, F. A. M.; Cohen Stuart, M. A.; van Well, A. A. *Langmuir* **1995**, *11*, 4467.

(8) (a) Zhu, J.; Lennox, R. B.; Eisenberg, A. *J. Phys. Chem.* **1992**, *96*, 4727. (b) Zhu, J.; Eisenberg, A.; Lennox, B. *J. Am. Chem. Soc.* **1991**, *113*, 5584.

(9) (a) Zeldin, M.; Wynne, K. J.; Allcock, H. R. *Inorganic and Organometallic Polymers*; ACS Symposium Series 360; American Chemical Society: Washington, DC, 1988. (b) Zeigher, J. M.; Fearon, F. W. G. *Silicon-Based Polymer Science*; Advances in Chemistry Series 224; American Chemical Society: Washington, DC, 1990. (c) Richard, J. G. *Silicon-Containing Polymers*; The Royal Society of Chemistry: Cambridge, 1995. (d) Kricheldorf, H. R. *Silicon in Polymer Synthesis*; Springer-Verlag: Berlin, 1996.

(10) (a) Matsumoto, K.; Yamaoka, H. *Macromolecules* **1995**, *28*, 7029. (b) Matsumoto, K.; Shimazu, H.; Deguchi, M.; Yamaoka, H. *J. Polym. Sci., Part A: Polym. Chem.* **1997**, *35*, 3207.

(11) (a) Matsumoto, K.; Deguchi, M.; Nakano, M.; Yamaoka, H. *J. Polym. Sci., Part A: Polym. Chem.* **1998**, *36*, 2699. (b) Matsumoto, K.; Wahnes, C.; Mouri, E.; Matsuoka, H.; Yamaoka, H. *J. Polym. Sci., Part A: Polym. Chem.* **2001**, *39*, 86.

(12) Knischka, R.; Frey, H.; Rapp, U.; Mayer-Posner, F. J. *Macromol. Rapid Commun.* **1998**, *19*, 455.

(13) Nakano, M.; Deguchi, M.; Matsumoto, K.; Matsuoka, H.; Yamaoka, H. *Macromolecules* **1999**, *32*, 7437.

(14) Nakano, M.; Deguchi, M.; Endo, H.; Matsumoto, K.; Matsuoka, H.; Yamaoka, H. *Macromolecules* **1999**, *32*, 6088.

(15) (a) Daillant, J., Gibaud, A., Eds.; *X-ray and Neutron Reflectivity: Principles and Apprecations*; Springer: Berlin, 1999. (b) Matsuoka, H.; Matsumoto, K.; Mouri, E. *Rigaku J.* **2001**, *18*, 54.

(16) Mori, H.; Wakasaka, O.; Hirao, A.; Nakahama, S. *Macromol. Chem. Phys.* **1994**, *195*, 3213.

(17) Ise, N.; Okubo, T.; Kunugi, S.; Matsuoka, H.; Yamamoto, K.; Ishii, Y. *J. Chem. Phys.* **1984**, *81*, 3294.

(18) (a) Yamaoka, H.; Matsuoka, H.; Kago, K.; Endo, H.; Eckelt, J. *Physica B* **1998**, *248*, 280. (b) Yamaoka, H.; Matsuoka, H.; Kago, K.; Endo, H.; Eckelt, J.; Yoshitome, R. *Chem. Phys.*

Lett. **1998**, *295*, 245. (c) Kago, K.; Matsuoka, H.; Endo, H.; Eckelt, J.; Yamaoka, H. *Supramol. Sci.* **1998**, *5*, 349. (d) Matsuoka, H.; Kago, K.; Yamaoka, H. *Rigaku-Denki J.* **1999**, *30*, 14.

(19) Sakurai, K. MUREX118: Program for calculation/analysis of X-ray reflectivity, fluorescence intensity from multi-layered thin films in grazing incident/exit X-ray experiments. National Research Institute for Metals, Tsukuba, Japan, 1995.

(20) Parratt, L. G. *Phys. Rev.* **1954**, *95*, 359.

(21) Sinha, S. K.; Sirota, E. B.; Garoff, S.; Stanley, H. B. *Phys. Rev. B* **1988**, *38*, 2297.

(22) Richter, D.; Schneider, D.; Monkenbusch, M.; Willner, L.; Fetters, L. J.; Huang, J. S.; Lin, M.; Mortensen, K.; Farago, B. *Macromolecules* **1997**, *30*, 1053.

(23) Matsuoka, H.; Yamamoto, Y.; Nakano, M.; Endo, H.; Yamaoka, H.; Zorn, R.; Monkenbusch, M.; Richter, D.; Seto, H.; Kawabata, Y.; Nagao, M. *Langmuir* **2000**, *16*, 9177.

(24) Guinier, A.; Fournet, G. *Small-Angle Scattering of X-rays*; John Wiley: New York, 1955.

(25) Nakano, M.; Matsumoto, K.; Matsuoka, H.; Yamaoka, H. *Macromolecules* **1999**, *32*, 4023.

(26) Sphere−rod transition of micelles formed by poly(ferrocenylsilane-*b*-dimethylsiloxane) in *n*-alkane, which is also considered to be driven by melting−crystallization of polyferrocenylsilane (micelle core segment) has recently been reported. Massey, J. A.; Temple, K.; Cao, L.; Rharbi, Y.; Raez, J.; Winnik, M. A.; Manners, I. *J. Am. Chem. Soc.* **2000**, *122*, 11577.

(27) Kiessig, H. *Ann. Phys.* **1931**, *10*, 769.

(28) The "beating" fringe in addition to "slow" fringe has also been reported for block copolymer films: de Jeu, W. H.; Lambooy, P.; Hamly, I. W.; Vaknin, D.; Pedersen, J. S.; Kjaer, K.; et al. *J. Phys. II* **1993**, *3*, 139.

(29) Kago, K.; Matsuoka, H.; Yoshitome, R.; Mouri, E.; Yamaoka, H. *Langmuir* **1999**, *15*, 4298.

(30) Kurian, P.; Zshoche, S.; Kennedy, J. P. *J. Polym. Sci., Part A: Polym. Chem.* **2000**, *38*, 3200.

MA011254N